AGU PUBLICATIONS

Geophysical Research Letters

RESEARCH LETTER
10.1002/2015GL063372

Key Points:
- ITCZ shift time scale increases linearly with model heat capacity
- Radiative feedbacks amplify ITCZ response to midlatitude heat flux forcing
- Equilibration time is 8 years for realistic slab-ocean mixed layer depth

Correspondence to:
M. D. Woelfle,
woelfle@atmos.washington.edu

Citation:
Woelfle, M. D., C. S. Bretherton, and D. M. W. Frierson (2015), Time scales of response to antisymmetric surface fluxes in an aquaplanet GCM, *Geophys. Res. Lett.*, *42*, doi:10.1002/2015GL063372.

Received 4 FEB 2015
Accepted 10 MAR 2015
Accepted article online 13 MAR 2015

Time scales of response to antisymmetric surface fluxes in an aquaplanet GCM

Matthew D. Woelfle[1], Christopher S. Bretherton[1], and Dargan M. W. Frierson[1]

[1]Department of Atmospheric Sciences, University of Washington, Seattle, Washington, USA

Abstract The intertropical convergence zone (ITCZ) shifts in response to hemispheric asymmetries in extratropical energy forcings. This study investigates the response time scale of this shift in an aquaplanet global climate model coupled to a slab ocean. A steady antisymmetric perturbation is abruptly added to the slab-ocean heat flux convergence in midlatitudes. The time scale of the ITCZ shift scales linearly with the heat capacity of the combined ocean-atmosphere system, and the shift is amplified by subtropical clear-sky radiation and cloud radiative feedbacks.

1. Introduction

The mean climate of the tropics is dominated by a pair of thermally direct circulation cells known as the Hadley circulation, with narrow regions of rising motion on their equatorward flank and broad subsidence regions extending toward the poles. The band of deep convection embedded in the rising branch is known as the intertropical convergence zone (ITCZ). Moisture converges into the ITCZ near the surface, and moist static energy is diverged aloft. Thus, the ITCZ is able to play a key role in regulating the interhemispheric energy distribution.

An early study using both observational data sets and simplistic models showed the mean latitude of the ITCZ in the west Atlantic to be sensitive to the local cross-equatorial sea surface temperature (SST) gradient, with the ITCZ shifting toward the warmer hemisphere [*Moura and Shukla*, 1981]. *Lindzen and Hou* [1988] explained the shifts by describing the ITCZ as an energy equator which predominantly fluxes energy into the cooler of the two hemispheres. A net energy flux into one hemisphere causes the ITCZ to shift toward that hemisphere which leads to increased net moist static energy flux into the less energetic hemisphere. This behavior has also been found in subsequent modeling studies of slowdowns in the Atlantic meridional overturning circulation (AMOC) [e.g., *Dong and Sutton*, 2002; *Chiang et al.*, 2008], climatological conditions during the Last Glacial Maximum [e.g. *Chiang et al.*, 2003; *Chiang and Bitz*, 2005; *Mahajan et al.*, 2011], artificial changes in surface heat fluxes [e.g., *Broccoli et al.*, 2006; *Kang et al.*, 2008, 2009, 2014; *Seo et al.*, 2014], and changes to other radiative forcing agents [*Yoshimori and Broccoli*, 2008, 2009].

Many of these studies also discuss the transient adjustment of the ITCZ to the imposed interhemispheric asymmetry. *Dong and Sutton* [2002] show the model equilibration time to changes in the AMOC and associated oceanic heat transport to be faster in a coupled atmosphere-ocean model, 7 years, as compared to an ocean-only model, decades. The authors also note changes in the ITCZ and tropical Atlantic SSTs as early as the fourth year after the AMOC is perturbed. Using a similar experimental setup, *Chiang et al.* [2008] note a change in the mean ITCZ latitude by the end of year 3, with the model reaching equilibrium in year 8. *Chiang and Bitz* [2005] report an ITCZ adjustment in a full atmospheric model coupled to a 50 m slab ocean beginning 15 months after an abrupt increase in Northern Hemisphere ice cover. *Mahajan et al.* [2011] show a similar response time scale when surface winds are held to their climatological control state. Using a full atmospheric model coupled to a 2.4 m slab ocean, *Kang et al.* [2014] show a midlatitude heat flux perturbation starts affecting the tropics 2 months after the initiation of the perturbation.

In this study, we use a full-physics atmospheric model coupled to a slab ocean of globally uniform depth to assess how fast the tropical climate responds to a sudden hemispherically asymmetric perturbation in extratropical heat fluxes. We vary the slab ocean's mixed layer depth from 2.4 m to 50 m to explore the impact of mixed layer depth on the adjustment time scale, and we diagnose the response mechanisms. The linearity of the response is tested by varying the amplitude of the heating anomaly. Section 2 describes the model configuration and experimental design. Section 3 describes the effect of mixed layer depth on

both the transients and resulting equilibria. Section 4 examines the mechanism by which the perturbed system adjusts to its new equilibrium. Section 5 summarizes these results and their implications.

2. Model and Methods

This study employs the Geophysical Fluid Dynamics Laboratory Atmospheric Model version 2.1 in aquaplanet configuration as described by *Anderson et al.* [2004]. The model has a horizontal resolution of 2° latitude × 2.5° longitude with 24 vertical levels. The atmospheric model is coupled to a nondiffusive slab ocean model with a prescribed heat capacity. The heat capacity of the slab ocean, C_{ocn}, is most readily described in terms of an equivalent mixed layer depth (MLD) for an isothermal layer of ocean water:

$$C_{ocn}(d) = \rho c_p d, \tag{1}$$

where ρ and c_p are the respective density and specific heat capacity of sea water and d is the equivalent mixed layer depth. This study utilizes slab oceans with heat capacities of approximately 1×10^7, 4.1×10^7, 10.3×10^7, and 20.6×10^7 J m^{-2} K^{-1} which correspond to MLDs d_{1-4} of 2.4, 10, 25, and 50 m, respectively. For comparison, the atmosphere has a heat capacity of approximately $C_{atm} = 1 \times 10^7$ J m^{-2} K^{-1}. The net energy flux that heats or cools the slab ocean is the sum of the net downward radiation, surface latent and sensible heat fluxes, melting of frozen precipitation, and an additional prescribed oceanic heat flux convergence which we refer to as the qflux. No sea ice is allowed to form in the model. SSTs are permitted to vary freely in order to maintain a closed energy budget. To simplify analysis of the transient response, the model is run under perpetual equinoctial conditions with no diurnal cycle.

The model is spun up for 10 years with a zonally uniform qflux equivalent to that used by *Frierson et al.* [2013], obtained by subtracting the zonal mean top of atmosphere (TOA) energy flux from the Clouds and the Earth's Radiant Energy System Energy Balanced and Filled satellite product [*Wielicki et al.*, 1996] from the ERA-Interim atmospheric energy divergence [*Dee et al.*, 2011] for the years 2001–2010. The prescribed qflux is meridionally asymmetric with greater energy input into the Northern Hemisphere, resulting in the ITCZ being located in the Northern Hemisphere. A 2.4 m mixed layer depth ocean is used during this initial period. Following the 10 year spin-up, the simulation is branched to four distinct simulations with mixed layer depths of 2.4, 10, 25, and 50 m. Each branch is perturbed by instantaneously adding to the control qflux an anomalous surface cooling in the Northern Hemisphere midlatitudes and heating in the Southern Hemisphere midlatitudes of a form similar to that used by *Kang et al.* [2008]:

$$H(\phi) = \begin{cases} -H_0 \sin\left(\frac{\phi+30}{30}\pi\right) & \text{for } -60 < \phi < -30 \\ -H_0 \sin\left(\frac{\phi-30}{30}\pi\right) & \text{for } 30 < \phi < 60 \\ 0 & \text{otherwise,} \end{cases} \tag{2}$$

where H_0 is the amplitude of the additional applied forcing and ϕ is latitude. Thus, the additional applied qflux serves as an implied oceanic heat flux, $F(\phi)$, from the Northern Hemisphere to the Southern Hemisphere, with no direct change in the global mean energy flux. The applied qflux and implied oceanic heat flux are related by $H = -\nabla \cdot F$. We prescribe the amplitude of H to correspond to an additional cross-equatorial heat flux of 1 PW southward. The prescribed modified qflux and associated implied heat transports are seen in Figure 1. The 2.4, 10, 25, and 50 m simulations are run for an additional 2, 5, 10, and 16 years, respectively, under the new forcing conditions. The unperturbed model is run from the branching point for an additional 4 years. The mean climate of the unperturbed model over this period is taken as the control for this investigation. Additional sensitivity simulations are performed using implied cross-equatorial heat fluxes of 0.5 PW and 2 PW southward.

As the response time scale is short for the shallowest MLD, we use daily model output in our analysis of the transient response. To reduce the impact of synoptic variability on our analysis, all daily output fields are zonally averaged. The zonal average at each latitude band is then temporally smoothed using a fourth-order, 20 day low-pass Butterworth filter to better isolate the large-scale response from the daily variability.

3. Response to Extratropical Heating

As expected, the removal of heat from the Northern Hemisphere along with concurrent addition of heat to the Southern Hemisphere leads to a smooth southward shift in the ITCZ, defined as the centroid of the

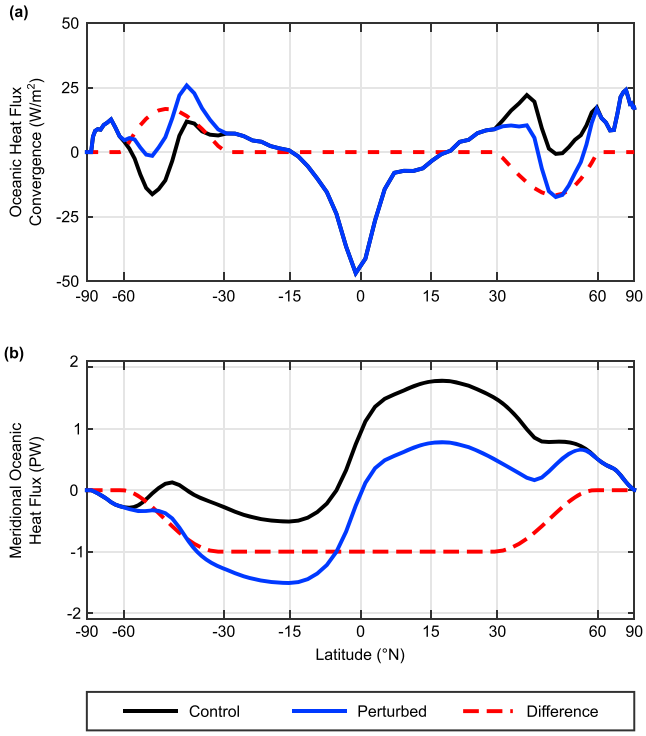

Figure 1. (a) Latitudinal structure of oceanic heat flux convergence, *H*, used in the control run (black) and in the perturbed flux run (blue). (b) Implied oceanic heat flux, *F*, for each prescribed oceanic heat flux convergence. Difference between runs shown in dashed red in each panel.

zonally averaged precipitation between 30°S and 30°N (Figures 2a–2d). In the control simulation, the ITCZ is located at 6°N. The ITCZ shifts to 3°S at equilibrium in the perturbed simulations.

In response to the perturbed forcing, the SST decreases in the Northern Hemisphere and increases in the Southern Hemisphere in all four simulations (Figures 2e–2h). However, the mean temperature response in the tropics and subtropics differs between the 2.4 m case and the deeper MLD cases. The equilibrium mean SST between 30°S and 30°N in the 2.4 m simulation is 300.8 K. The control simulation, which was performed with a 2.4 m MLD, has the same mean SST in this region. The simulations with greater MLDs show an equilibrium mean surface temperature 1.2 to 1.5 K larger than this. They also have a smaller mean low-cloud fraction in the tropics and subtropics (0.33) than for the 2.4 m simulation (0.39). Thus, we suspect a rectified transient coupling between the low cloud and the differing MLDs to be the driver of this SST difference. Since this difference is not central to our study, it was not investigated further. The equilibrium mean SST poleward of the subtropics is similar across the simulations.

The transient surface temperature and precipitation responses in Figure 2 are plotted with the time axis of each panel scaled by the heat capacity of the respective modeling system. When scaled in this manner, the transient responses of the four differing MLD simulations are strikingly similar, suggesting the response time scale of the four simulations are a linear function of the total heat capacity of the ocean-atmosphere system. For the mixed layer depth d_i, the system heat capacity C_i is

$$C_i = C_{\mathrm{ocn}}(d_i) + C_{\mathrm{atm}} = (2, 5.1, 11.3, 21.6),\ i = 1, \ldots, 4. \tag{3}$$

Here C_i is given in units of 10^7 J m^{-2} K^{-1}. To test the linearity of the response, we define a scaled time relating the actual elapsed time and the model's heat capacity for each MLD:

$$\hat{t} = t/C_i, \tag{4}$$

where t is the actual time after the flux perturbation. Thus, for the 2.4 m simulation, the scaled time is half the actual time, while for the 50 m simulation, it is approximately 5% of the actual time. In this study, we compute equilibrium quantities for the perturbed flux simulations by averaging all output beyond a scaled time of 250 d/(J m^{-2} K^{-1}), which corresponds to 500 d for the 2.4 m MLD but over 14 years for the 50 m MLD.

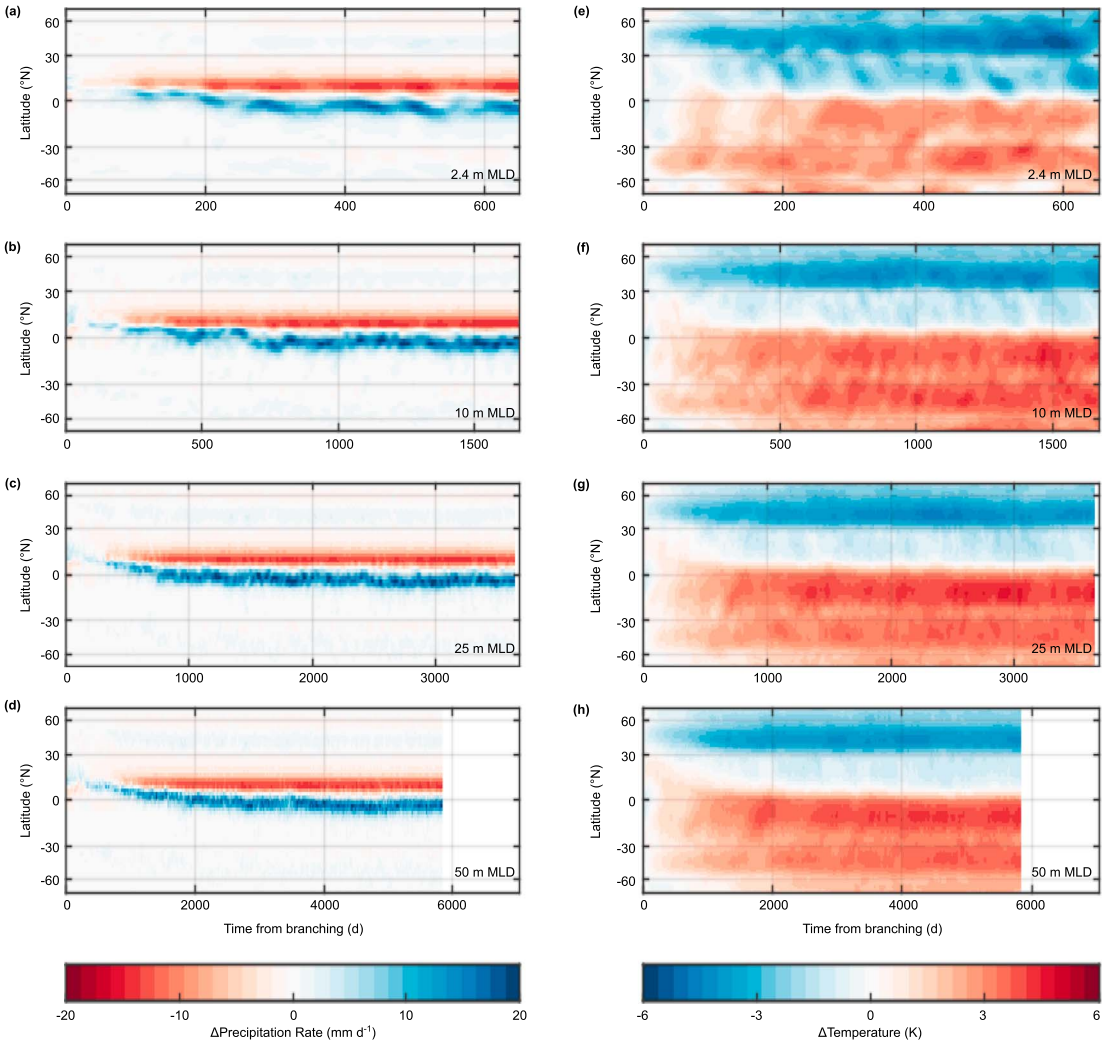

Figure 2. Zonal average (a–d) precipitation and (e–h) surface temperature response to altered surface flux at various mixed layer depths. Values shown are the zonal average of the perturbed flux run minus the temporal and zonal mean of the control run.

We characterize the model's transient response to the anomalous heating using the tropical SST asymmetry, A^T, defined as the mean SST between 0°N and 20°N minus the mean SST between 0°S and 20°S [*Hwang and Frierson*, 2013]. *Hwang and Frierson* [2013] showed this metric to be well correlated with the location of the ITCZ in the Coupled Model Intercomparison Project Phase 5 archive. Unlike tropical SST, the equilibrium tropical SST asymmetry is fairly consistent across the simulations with asymmetries of −1.4, −1.5, −1.6, and −1.3 for the 2.4, 10, 25, and 50 m MLD simulations, respectively. Thus, it is still appropriate to use the transient tropical surface temperature asymmetry to characterize the time scale of the modeled tropical response despite the differences in mean SST response.

To account for differences in the equilibrium response between the simulations, the asymmetry is normalized as follows:

$$A^T_{\text{norm}} = \frac{A^T - A^T_{\text{eq}}}{A^T_{\text{ctrl}} - A^T_{\text{eq}}}, \tag{5}$$

where A^T_{norm} is the normalized tropical SST asymmetry, A^T is the daily averaged transient asymmetry, A^T_{eq} is the equilibrium asymmetry for the modified qflux simulation, and A^T_{ctrl} is the asymmetry for the control simulation. A normalized asymmetry of one corresponds to the mean control run asymmetry, and a normalized asymmetry of zero corresponds to the mean equilibrium asymmetry of the perturbed flux simulation.

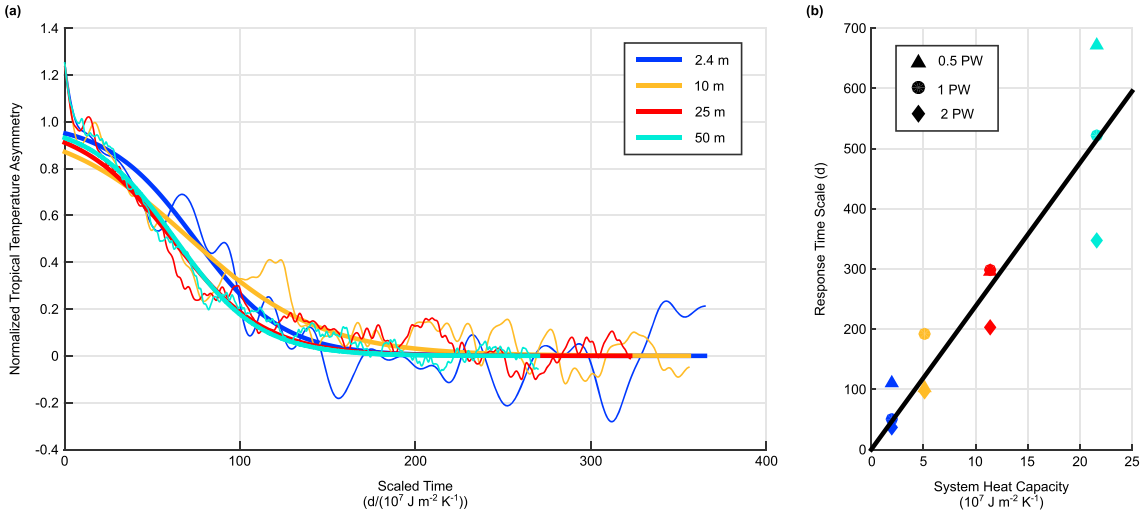

Figure 3. (a) Transient normalized tropical surface temperature asymmetry versus scaled time $\hat{t} = t/C$ for the 1 PW cross-equatorial perturbation case where C is the total column heat capacity in units of 10^7 J m^{-2} K^{-1} (thin line). Also shown is the logistic fit to each transient (thick line). (b) Time scale τ derived from the logistic fit for all simulations as a function of total heat capacity C, along with a least squares fit line for all points that passes through the origin.

Following normalization, each transient asymmetry is fit with a two parameter logistic function of the form:

$$\hat{A}^T = \left[1 + \exp\left(\frac{t - t_o}{\tau}\right)\right]^{-1}, \tag{6}$$

where $\hat{A}^T$ is the fit to the normalized asymmetry, t is the time from branching, and t_o and τ are the fit parameters. The response time scale of each model configuration is measured by τ.

The normalized transient tropical temperature asymmetry is plotted against scaled time for each of the four MLDs in Figure 3a. As expected from the similarity of the responses shown in Figure 2, the transient asymmetries for each simulation are nearly identical across MLD with this time scaling. Each transient shows a slow initial response as the perturbed heating forces changes in the extratropics which are not yet communicated to the tropics. By scaled day 25, the midlatitude response to the anomalous qflux begins to propagate into the tropics. There, dynamic and radiative feedbacks communicate the signal across the tropics leading to a rapid change in the normalized tropical temperature asymmetry. Details of this adjustment are provided in section 4. As the system approaches equilibrium, the rate of response slows. By scaled day 250, all of the simulations have reached their new equilibrium state.

As described above, a logistic function is fit to the normalized temperature asymmetry response (Figure 3a). The time scale parameter, τ, for each logistic fit, including the halved and doubled amplitude simulations, is plotted against its respective modeling system's equivalent oceanic mixed layer depth in Figure 3b. A linear fit to all points is included for this panel where the y intercept is forced to be zero as a system with near-zero heat capacity would be expected to respond instantaneously to any external forcing. By visual inspection, it can be seen that the points lie roughly along this line, with the response of time 2 PW simulations being faster than the other simulations, particularly for the two deepest MLDs. The differing responses are likely tied to the differences in cloud feedbacks as discussed in the following section. For the shallowest mixed layer depth of 2.4 m and a 1 PW cross-equatorial flux perturbation, the adjustment time scale is 50 days. For a more realistic mixed layer depth of 50 m, the adjustment time scale is much longer, 522 days. Using this time scale, the time necessary to reach a given percentage of the way to the new equilibrium can be computed as

$$t = t_o + \tau \ln\left(\frac{\gamma}{1 - \gamma}\right), \tag{7}$$

where γ is the fractional approach to equilibrium. For the 50 m mixed layer simulation, the model reaches 95% of its new equilibrium value in just under 8 years. The second fit parameter, t_o, marks the point at which the perturbed simulation is approximately halfway to its new equilibrium. The relationship between t_o and

MLD is also strongly linear for a given forcing amplitude (not shown). We next explore the mechanism for the extratropically forced tropical response.

4. Column Energy Balance Response

The location of the ITCZ has been shown to be dependent on the interhemispheric contrast in vertically integrated moist static energy [*Kang et al.*, 2008]. Thus, we examine the column energy budget for the model to further understand the processes behind the tropical precipitation and circulation changes. The full model column is used in place of the atmospheric column because of the strong surface flux coupling between atmosphere and ocean. The SST responds to transient imbalance between the qflux and the surface energy flux from ocean to atmosphere and provides most of the thermal inertia in the column, while the atmosphere responds to the surface flux. Once equilibrium is reached, the applied qflux modification will drive an anomalous surface energy flux to the atmosphere, where it will be removed by diabatic processes and circulation changes.

The zonally averaged column energy budget consists of radiative fluxes at the top of atmosphere, R_{TOA}, the qflux into the slab ocean, and meridional atmospheric energy transports as follows:

$$\frac{\mathrm{d}E_{\mathrm{col}}}{\mathrm{d}t} = R_{\mathrm{TOA}} + \mathrm{qflux} - [v] \cdot \nabla[\mathrm{MSE}], \tag{8}$$

where $[v]$ is the vertically integrated meridional wind speed and the column energy, E_{col}, is the sum of the vertically integrated atmospheric moist static energy, [MSE], and the oceanic thermal energy, E_{ocn}

$$E_{\mathrm{col}} = [\mathrm{MSE}] + E_{\mathrm{ocn}}(T). \tag{9}$$

We use model outputs of specific humidity, temperature, and geopotential height to compute atmospheric moist static energy. The oceanic thermal energy is obtained by multiplying the SST by the oceanic heat capacity. The meridional atmospheric energy transport is computed as the residual of equation (8). Figure 4 shows the equilibrium response of the TOA radiative fluxes and atmospheric energy transport as a difference between the equilibrated 2.4 m MLD simulation ($\hat{t} > 250$ d) and the mean of the control simulation. Positive values for the fluxes indicate net sources of energy into the model column. The other three MLD simulations show qualitatively similar adjustments.

As is expected from the structure of the additional qflux, the changes in column energy are first manifest in the midlatitudes. The applied qflux change forces SSTs in the Northern Hemisphere midlatitudes to decline. The surface cooling is communicated to the atmosphere through a reduction in both surface latent heat flux and upwelling longwave radiation. Cooling the atmospheric column leads to a decrease in outgoing TOA clear-sky longwave radiation due to the reduced emission temperature. This has a warming effect on the model column that opposes the decreased oceanic heat flux convergence. Water vapor is reduced in the Northern Hemisphere middle and high latitudes, but the resulting radiative effect is small compared to the strength of the Planck feedback in this region. By contrast, the changes in water vapor dominate the Planck feedback in the subtropics and tropics. Reduced water vapor allows more outgoing longwave radiation in the Northern Hemisphere within these latitudes, with an antisymmetric response in the Southern Hemisphere. *Seo et al.* [2014] show the location of the applied perturbation to control the balance between the positive low-latitude and negative high-latitude feedbacks. In the simulations presented here, changes in clear-sky radiation from the control simulation contribute 1.7 W m^{-2} more energy into the Southern Hemisphere than the Northern Hemisphere. Thus, TOA clear-sky radiation is a positive feedback on the ITCZ shift. As no sea ice is allowed to form, the ice-albedo feedback is not represented in these simulations. However, we expect this feedback would lead to reduced (enhanced) net downward radiation in the Northern (Southern) Hemisphere further amplifying the asymmetry of the clear-sky radiative response and the simulated ITCZ shift.

We will interpret the change in TOA cloud radiative effect as a feedback of cloud changes on the ITCZ shift; this neglects the slight "masking" contribution to the cloud radiative response associated with a fixed cloud cover reducing the radiative effects of a water vapor change [*Soden et al.*, 2004]. Within the Northern Hemisphere midlatitudes, the cloud radiative response is driven by the shortwave response to increased total cloud cover. In the Northern Hemisphere subtropics, the model simulates a reduction in high cloud fraction which has little net radiative effect as the resulting shortwave and longwave responses largely

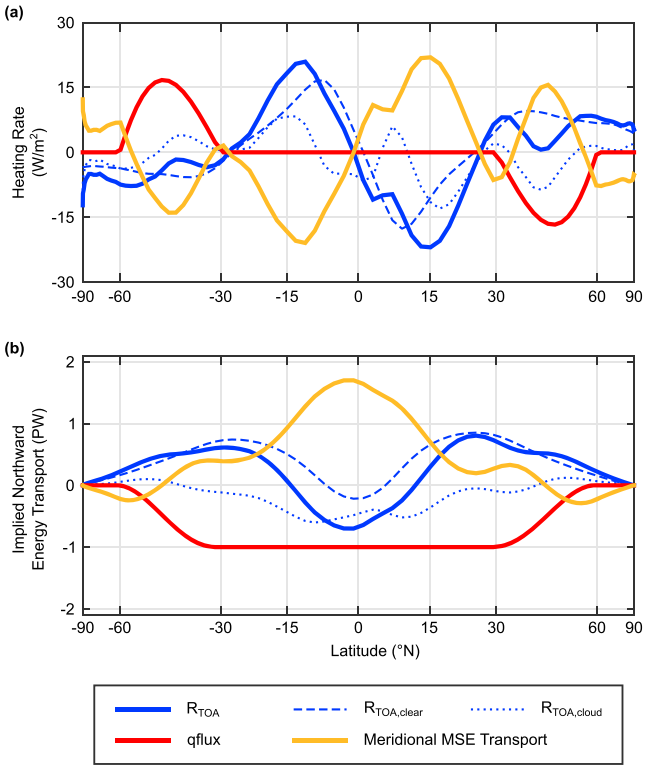

Figure 4. Equilibrium response of the zonally averaged (a) local column heating rates and (b) implied energy transports for the 2.4 m mixed layer simulation. Values shown are the difference between the mean of the equilibrated perturbed flux run and the mean of the control run. Positive values in Figure 4a indicate heating rate changes which have a warming effect on the atmospheric column.

cancel. The net cloud radiative response in this region is driven by increased low cloud cover which reduces net downwelling shortwave radiation and has a negligible longwave response. The extratropical and subtropical features are relatively antisymmetric between hemispheres. However, this is not true of the deep tropics. In the Northern Hemisphere, the change in cloud radiative effect produces a narrow band of warming north of the original ITCZ location with cooling south of this latitude. In the Southern Hemisphere, the cloud radiative response yields a net cooling through the deep tropics. Though the sign of the net cloud radiative feedback is again dependent on the location of the applied perturbation [*Seo et al.*, 2014], in these simulations, the cloud radiative response is a positive feedback on the ITCZ shift. The cloud effect on radiation allows 3.7 W m^{-2} more energy into the Southern Hemisphere than the Northern Hemisphere in the 2.4 m MLD simulation. The amplitude of the radiative changes varies across MLDs, but the sign of the feedback is uniformly positive across the simulations.

The residual of the column energy budget is interpreted to be the meridional atmospheric energy transport. As expected by the ITCZ shift, this term serves to transport 1.7 PW of heat northward from the warmed Southern Hemisphere into the Northern Hemisphere in the 2.4 m MLD simulation. This is greater than that expected simply from the qflux perturbation due to the positive feedback of TOA radiation on the response.

The simulations with halved and doubled qflux perturbations show the net positive cloud feedback to increase in strength with increasing perturbation magnitude mainly due to increased subtropical cloud feedbacks. The amplification of this feedback is likely responsible for the quickened response time scale seen in Figure 3b for the 2 PW forcing case. The net clear-sky radiative feedback remains weakly positive for all perturbation amplitudes.

5. Discussion and Conclusions

In this study, we examine the transient response of a full-physics atmospheric climate model coupled to a slab ocean of uniform depth. We perturb the model by suddenly turning on a source of heat to the slab

ocean in the Southern Hemisphere midlatitudes and removing the same amount of heat from the Northern Hemisphere midlatitude slab ocean. Heating the Southern Hemisphere and cooling the Northern Hemisphere raises southern hemispheric temperatures, decreases northern hemispheric temperatures, and after some time, shifts the mean location of the ITCZ southward. The response time scale is found to scale linearly with the column heat capacity of the slab ocean and atmosphere combined, ranging from 50 days for a simulation with a 2.4 m thick oceanic mixed layer depth to over 10 times as long for a 50 m MLD. Utilizing the derived time scale, the 50 m mixed layer simulation is shown to be 50% of the way to its new equilibrium after 3.7 years and 95% of the way to its new equilibrium after 7.9 years, which is consistent with the adjustment time scale noted for fully coupled models responding to changes in AMOC [*Dong and Sutton*, 2002; *Chiang et al.*, 2008]. This response time is long compared to the time for east Pacific double ITCZ precipitation biases to develop in some coupled models initialized from observed or nonequilibrium conditions [*Liu et al.*, 2012], suggesting the transient development of double ITCZ biases in coupled models with realistic geography may help separate remote midlatitude contributions from biases induced by local processes such as cumulus convection or cloud cover.

We also examine the mechanisms of the response. The midlatitude oceanic heat flux convergence changes are communicated to the atmosphere primarily through changes in surface latent heat flux and upwelling longwave radiation. Both clear-sky and cloud radiative effects are positive feedbacks on the applied oceanic heat flux convergence modification, with cloud feedbacks becoming more strongly positive as the forcing amplitude is increased. These response mechanisms are consistent with prior work and confirm the importance of cloud and radiation feedbacks in the tropical response to extratropical forcings.

Acknowledgments

The authors would like to thank Elizabeth Maroon for her assistance with the AM2.1, John Fasullo for providing the ERA-Interim divergence data, and Tony Broccoli and one anonymous reviewer for their feedback on this manuscript. Matthew Woelfle was supported by the Department of Defense (DoD) through the National Defense Science and Engineering Graduate Fellowship (NDSEG) Program. Bretherton acknowledges support from NSF grant AGS-1419507. Frierson was supported by NSF grants AGS-0846641, AGS-0936059, AGS-1359464, PLR-1341497, and a UW Royalty Research Fund grant. Model output used in this study is available upon request to Matthew Woelfle (woelfle@atmos.washington.edu).

The Editor thanks Anthony J. Broccoli and an anonymous reviewer for their assistance in evaluating this paper.

References

Anderson, J. L., et al. (2004), The new GFDL global atmosphere and land model AM2-LM2: Evaluation with prescribed SST simulations, *J. Clim.*, *17*(24), 4641–4673, doi:10.1175/JCLI-3223.1.

Broccoli, A. J., K. A. Dahl, and R. J. Stouffer (2006), Response of the ITCZ to northern hemisphere cooling, *Geophys. Res. Lett.*, *33*, L01702, doi:10.1029/2005GL024546.

Chiang, J. C. H., and C. M. Bitz (2005), Influence of high latitude ice cover on the marine intertropical convergence zone, *Clim. Dyn.*, *25*(5), 477–496, doi:10.1007/s00382-005-0040-5.

Chiang, J. C. H., M. Biasutti, and D. S. Battisti (2003), Sensitivity of the Atlantic intertropical convergence zone to last glacial maximum boundary conditions, *Paleoceanography*, *18*(4), 1094, doi:10.1029/2003PA000916.

Chiang, J. C. H., W. Cheng, and C. M. Bitz (2008), Fast teleconnections to the tropical Atlantic sector from Atlantic thermohaline adjustment, *Geophys. Res. Lett.*, *35*, L07704, doi:10.1029/2008GL033292.

Dee, D. P., et al. (2011), The ERA-Interim reanalysis: Configuration and performance of the data assimilation system, *Q. J. R. Meteorol. Soc.*, *137*(656), 553–597, doi:10.1002/qj.828.

Dong, B.-W., and R. T. Sutton (2002), Adjustment of the coupled ocean-atmosphere system to a sudden change in the thermohaline circulation, *Geophys. Res. Lett.*, *29*(15), 1728, doi:10.1029/2002GL015229.

Frierson, D. M. W., Y.-T. Hwang, N. S. Fučkar, R. Seager, S. M. Kang, A. Donohoe, E. Maroon, X. Liu, and D. S. Battisti (2013), Contribution of ocean overturning circulation to tropical rainfall peak in the Northern Hemisphere, *Nat. Geosci.*, *6*(11), 940–944, doi:10.1038/ngeo1987.

Hwang, Y.-T., and D. M. W. Frierson (2013), Link between the double-intertropical convergence zone problem and cloud biases over the Southern Ocean, *Proc. Natl. Acad. Sci.*, *110*(13), 4935–4940, doi:10.1073/pnas.1213302110.

Kang, S. M., I. M. Held, D. M. Frierson, and M. Zhao (2008), The response of the ITCZ to extratropical thermal forcing: Idealized slab-ocean experiments with a GCM, *J. Clim.*, *21*(14), 3521–3532, doi:10.1175/2007JCLI2146.1.

Kang, S. M., D. M. W. Frierson, and I. M. Held (2009), The tropical response to extratropical thermal forcing in an idealized GCM: The importance of radiative feedbacks and convective parameterization, *J. Atmos. Sci.*, *66*(9), 2812–2827, doi:10.1175/2009JAS2924.1.

Kang, S. M., I. M. Held, and S.-P. Xie (2014), Contrasting the tropical responses to zonally asymmetric extratropical and tropical thermal forcing, *Clim. Dyn.*, *42*(7–8), 2033–2043, doi:10.1007/s00382-013-1863-0.

Lindzen, R. S., and A. V. Hou (1988), Hadley circulations for zonally averaged heating centered off the equator, *J. Atmos. Sci.*, *45*(17), 2416–2427, doi:10.1175/2009JAS2924.1.

Liu, H., M. Zhang, and W. Lin (2012), An investigation of the initial development of the double-ITCZ warm SST biases in the CCSM, *J. Clim.*, *25*, 140–155, doi:10.1175/2011JCLI4001.1.

Mahajan, S., R. Saravanan, and P. Chang (2011), The role of the Wind-Evaporation-Sea Surface Temperature (WES) feedback as a thermodynamic pathway for the equatorward propagation of high-latitude sea ice-induced cold anomalies, *J. Clim.*, *24*(5), 1350–1361, doi:10.1175/2010JCLI3455.1.

Moura, A. D., and J. Shukla (1981), On the dynamics of droughts in northeast Brazil: Observations, theory and numerical experiments with a general circulation model, *J. Atmos. Sci.*, *38*(12), 2653–2675, doi:10.1175/1520-0469(1981)038<2653:OTDODI>2.0.CO;2.

Seo, J., S. M. Kang, and D. M. W. Frierson (2014), Sensitivity of intertropical convergence zone movement to the latitudinal position of thermal forcing, *J. Clim.*, *27*(8), 3035–3042, doi:10.1175/JCLI-D-13-00691.1.

Soden, B. J., A. J. Broccoli, and R. S. Hemler (2004), On the use of cloud forcing to estimate cloud feedback, *J. Clim.*, *17*(19), 3661–3665, doi:10.1175/1520-0442(2004)017<3661:OTUOCF>2.0.CO;2.

Wielicki, B. A., B. R. Barkstrom, E. F. Harrison, R. B. Lee, G. Louis Smith, and J. E. Cooper (1996), Clouds and the Earth'S Radiant Energy System (CERES): An Earth observing system experiment, *Bull. Am. Meteorol. Soc.*, *77*(5), 853–868, doi:10.1175/1520-0477(1996)077<0853:CATERE>2.0.CO;2.

Yoshimori, M., and A. J. Broccoli (2008), Equilibrium response of an atmosphere-mixed layer ocean model to different radiative forcing agents: Global and zonal mean response, *J. Clim.*, *21*(17), 4399–4423, doi:10.1175/2008JCLI2172.1.

Yoshimori, M., and A. J. Broccoli (2009), On the link between Hadley circulation changes and radiative feedback processes, *Geophys. Res. Lett.*, *36*, L20703, doi:10.1029/2009GL040488.